

Two functionals approach in DFT for the prediction of thermoelectric properties of Fe_2ScX ($X = \text{P, As, Sb}$) full Heusler compounds

Shivprasad S. Shastri* and Sudhir K. Pandey†

School of Engineering, Indian Institute of Technology Mandi, Kamand - 175005, India

(Dated: April 10, 2019)

In the quest of new thermoelectric materials with high power factors, full-Heusler compounds having flat band are found to be promising candidates. In this direction, Fe_2ScX ($X=\text{P,As,Sb}$) compounds are investigated using mBJ for the band gap and SCAN to describe the electronic bands and phonon properties for thermoelectric applications. The band gaps obtained from mBJ are 0.81 eV, 0.69 eV and 0.60 eV for Fe_2ScX compounds, respectively. The phonon dispersion, phonon density of states (DOS) and partial DOS are calculated. The phonon contributions to specific heat are obtained as a function of temperature under harmonic approximation. The electronic band structure calculated from mBJ and SCAN functionals are qualitatively compared. The effective mass values are calculated at the band extrema from SCAN functional. The thermoelectric parameters are calculated for both hole and electron dopings under semiclassical theory. We use simple, but reasonable method to estimate the phonon relaxation time (τ_{ph}). Using the specific heat, estimated τ_{ph} and slopes (phase velocity) of acoustic branches in the linear region, lattice thermal conductivity (κ_{ph}) at 300 K is calculated for three compounds. The obtained values of κ_{ph} with constant τ_{ph} are 18.2, 13.6 and 10.3 $\text{Wm}^{-1}\text{K}^{-1}$, respectively. Finally, the temperature dependent figure of merit ZT values are calculated for optimal carrier concentrations in the doping range considered, to evaluate the materials for thermoelectric application. The ZT values for n-type Fe_2ScX , in 900-1200 K, are 0.34-0.43, 0.40-0.48 and 0.45-0.52, respectively. While, the p-type Fe_2ScX have ZT of 0.25-0.34, 0.20-0.28 and 0.18-0.26, respectively in the same temperature range. The ZT values suggest that, Fe_2ScX compounds can be promising materials in high temperature power generation application on successful synthesis and further κ_{ph} reduction by methods like nanostructuring.

I. INTRODUCTION

The development of materials which can extract the heat energy and transform it into electrical energy is an important area of research.^{1,2} Since, devices made out of such materials can be installed at automobile heat generating parts, to convert the industrial waste heat, in home heating appliances, etc. Those materials are termed thermoelectric (TE) materials and device fabricated using them are called thermoelectric generators (TEG).³ Research in the area of developing TE materials is important since they can be a very good alternative energy sources in many small scale applications. TEGs are green energy sources compared to the conventional fossil fuel based energy sources. The TE materials with dimensionless figure of merit $ZT \geq 1.0$ are considered as suitable for TE applications. But, the bottle neck in implementing the most of the existing TE materials into technological applications is due to their poor value of ZT . Therefore, there has been continuous efforts in TE area of research to enhance the efficiency as well as in searching for new TE materials.

Efficiency of a thermoelectric can be increased by maximizing its electrical power and by reducing the heat transport by electrons and phonons. The electrical power depends on the electrical conductivity, σ , and Seebeck coefficient, S , of the material.³ The transport of heat in a material is decided by the electronic and phonon contributions to thermal conductivity. Thus, in order to have a thermoelectric with high figure of merit, given by the

relation,

$$ZT = \frac{S^2 \sigma T}{\kappa} \quad (1)$$

the power factor, $S^2 \sigma$ must be higher and thermal conductivity $\kappa = \kappa_e + \kappa_{ph}$ should be lower. The thermal conductivity κ in a material is a sum of electronic and lattice part of thermal conductivities denoted by κ_e and κ_{ph} , respectively. Many methods like alloying, nanostructuring are employed to reduce the lattice thermal conductivity by increasing phonon scattering without or least affecting its electronic structure.⁴ Another method towards improving efficiency is to improve the power factor of the material. The power factor of a material is mainly decided by its electronic structure and such materials are being searched which could have electronic structure that yields high power factor.⁵

The studies of electronic structure and thermoelectric properties carried out on many Heusler alloys suggested that, they possess a flat conduction band along $\Gamma - X$ direction and hence larger effective mass of carriers and higher Seebeck coefficient values.⁶⁻⁹ These works suggested that full-Heusler alloys with a semiconducting ground states could be used for thermoelectric applications. Sharma *et al.*¹⁰ reported three new full-Heusler alloys having flat conduction band *viz.* Fe_2ScP , Fe_2ScAs and Fe_2ScSb with their electronic structure and thermoelectric properties using density functional theory (DFT) calculations. In a DFT calculation, generally band gaps are underestimated and Fe_2ScSb compound in the work of Ref.10 was predicted to be a semimetal. The transport

coefficients to be calculated in first-principles calculations are highly dependent on the band gap and band structure of the compound. The electronic structure changes depending on the exchange-correlation (XC) functional used in the DFT calculations. Therefore, in the computational discovery of thermoelectric materials, selection and benchmarking of XC functional becomes an important step.

In our previous work¹¹, electronic structure of two iron based Heusler alloys Fe₂VAl and Fe₂TiSn were studied using five XC functionals. The effective mass values estimated showed the dependence of band features on XC functionals and usefulness of mBJ in predicting accurate band gaps providing a bench mark study. In semiconductors and insulators, transport of heat is mainly through the phonons and thus study of phonon properties is important to understand the thermal conductivity. The phonon calculations are useful in extracting information about stability of the crystal, lattice contribution to specific heat and other thermal properties, and thermal expansion of crystals. A computational study of phonon dispersion of a material along with its electronic structure would completely describe TE material which makes phonon calculations, desirable in a study of TE properties. Recently, in the work of Shamim *et al.*,¹² the Seebeck coefficient S value of Fe₂VAl was measured in the range 300-620 K. This experimental S values were explained using DFT and Boltzmann transport calculations using different XC functionals. The best matching between the experimental and theoretical values was found, for using the band gap obtained from mBJ and band structure from SCAN or PBEsol. Therefore, motivated by the results of the work of Shamim *et al.*¹², we investigate the electronic structure and thermoelectric properties of the Fe₂ScX (X=P, As, Sb) compounds.

To investigate the electronic structure and dependent properties mBJ and SCAN functionals are used. Using the mBJ, band gaps of 0.81, 0.69 and 0.60 eV are obtained for Fe₂ScX (X=P, As, Sb) compounds, respectively. Using SCAN, phonon dispersion, total density of states (DOS) and partial DOS are also calculated. The specific heat contribution from the lattice part of compounds are calculated. The Debye temperatures estimated from the highest phonon frequency for three compounds are ~ 637 K, ~ 556 K and ~ 498 K, respectively. Seebeck coefficient, electrical conductivity per relaxation time, power factor per relaxation time and electronic thermal conductivity per relaxation time are calculated with temperature for different values of electron and hole dopings. The effective mass values are calculated at the band extrema. The electronic band structures obtained from mBJ and SCAN are qualitatively compared. We make use of simple method in this work to estimate phonon relaxation time τ_{ph} . Using calculated specific heat, τ_{ph} and slopes of acoustic branches in the linear region close to Γ , κ_{ph} values at 300 K are calculated. Then to further evaluate the material for TE applications, we calculate temperature dependent ZT for

three compounds for the highest power factor giving electron and hole doping concentrations.

II. COMPUTATIONAL DETAILS

In our work, full-potential linearized augmented plane wave (FP-LAPW) method based first-principles DFT program WIEN2k¹³ is used for the calculation of ground state energy, electronic structure and total forces on atoms. mBJ exchange potential with LDA correlation¹⁴ and SCAN¹⁵ exchange-correlation functionals are chosen for the calculations. Here, The lattice parameters are taken from the Ref. 10 and used for electronic properties calculation. Since, phonon frequency is sensitive to the lattice parameter, it is optimized for force calculations with SCAN functional. For force constants and phonon properties calculations phonopy¹⁶ code is used. Phonon properties are calculated under finite displacement method (FDM) and supercell approach in phonopy. To capture the long-range force constant between atoms a supercell of size $2 \times 2 \times 2$ with 128 atoms is constructed. To create the forces artificially in the system each of inequivalent atoms in the formula unit of Fe₂ScX is displaced by 0.02 Bohr in x-direction. To obtain the forces on the atoms in the created supercell, force convergence criteria of 0.1mRy/Bohr is set in the force calculator (WIEN2k). A k-mesh of size $5 \times 5 \times 5$ is used for the force calculations in supercell. The calculations of band structure dependent transport coefficients are done using BoltzTraP program.¹⁷ The ground state total energy calculations are done on dense k-mesh of $50 \times 50 \times 50$ size in order to facilitate transport calculations. The convergence criteria to meet the self-consistency in iterations for total energy 10^{-4} Ry/cell and for charge/cell is 10^{-2} electronic charges, respectively are used.

III. RESULTS AND DISCUSSION

We built the crystal structure of Fe₂ScX (X=P, As, Sb) full-Heusler compounds in the cubic L2₁ phase with space group $Fm-3m$ ¹⁰. In Ref. 10 the ground state formation energy of the static lattices have been calculated. The obtained negative values of formation energies supported the feasibility of synthesis of Fe₂ScX (X=P, As, Sb) in laboratories. Further, to study the structural stability of the compounds we have carried out phonon calculations. The phonon frequencies are sensitive to lattice parameter and exchange-correlation functional¹⁸ used in the computation (which was also observed in our previous work.¹⁹) Therefore, the lattice parameters taken from Ref. 10 were optimized to get the ground state lattice parameters for SCAN functional. The equilibrium lattice parameters after fitting the B-M EOS²⁰ for the energy-volume curves are 5.704, 5.828, and 6.085 Å for Fe₂ScP, Fe₂ScAs and Fe₂ScSb, respectively. Using these lattice parameters from SCAN phonon dispersion, den-

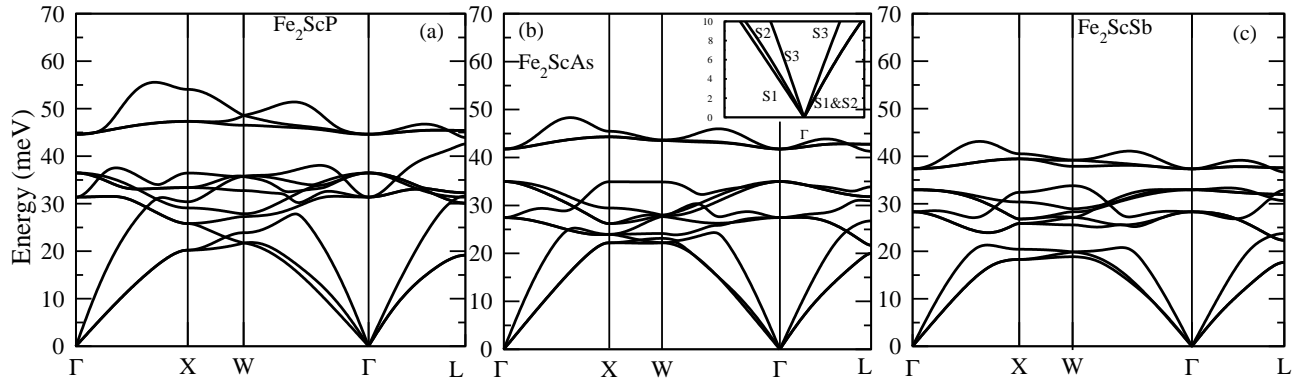


FIG. 1: Phonon dispersion curves of Fe_2ScP , Fe_2ScAs and Fe_2ScSb .

sity of states (DOS) and electronic dispersions are studied.

A. Phonon properties

The phonon dispersions for Fe_2ScX ($X=\text{P, As, Sb}$) compounds are presented in Fig. 1(a) to (c). The calculated phonon spectrum does not show any negative frequency (or energy) which suggests that crystal is stable for any small atomic displacements about the mean position. Dynamical stability of the compounds found out with phonon calculations and formation energy values from Ref. 10 further supports the possibility of preparation of samples in laboratories.

In the figure, one can observe that maximum phonon energy is decreasing from Fe_2ScP to Fe_2ScSb . The highest energy phonons are of ~ 55 , ~ 48 and ~ 43 meV for Fe_2ScP , Fe_2ScAs and Fe_2ScSb , respectively. The observed decreasing trend in phonon frequency can be mainly due to the following reasons. The radius of atoms X (P, As, Sb) in the unit cell of Fe_2ScX is increasing from P to Sb making distance between atoms and hence, the lattice constant to increase from Fe_2ScP to Fe_2ScSb . Also, the X atoms in the unit cell are heavier in mass on going from P to Sb. Since, the mass of atoms and distance between them are increased the frequency of vibrations of atoms is expected to reduce from first to last compound in the Fe_2ScX family. The phonon properties and electronic structure for Fe_2ScAs are discussed in our earlier work²¹ but, to study the family of Fe_2ScX with $X = \text{P, As, Sb}$ atoms for thermoelectric applications, we included Fe_2ScAs here, for the purpose of completeness in the discussion.

The phonon dispersion for Fe_2ScP in Fig. 1 (a) shows three acoustic branches, out of which one branch is degenerate with optical branch at k-points nearer to X-point in the Γ -X direction. Three optical branches starting at 45 meV are well separated from the rest of the branches along the k-path directions shown in the plot except near L-point, around 43 meV, where the separation is very much reduced (~ 0.14 meV). This separation

is also noted in the dispersions of Fe_2ScAs and Fe_2ScSb . In Fe_2ScAs above 40 meV and in Fe_2ScSb above 35 meV optical branches with clear separation are situated. In case of Fe_2ScSb , optical and acoustic branches are touching only near L-point at ~ 22 meV unlike in other two compounds. From phonon dispersion we can also observe that the maximum energy for acoustic phonons in a given compound is reducing from Fe_2ScP to Fe_2ScSb .

Fig. 2(a)-(c) and (d)-(f) show the calculated phonon total density of states (TDOS) and partial DOS for Fe_2ScX ($X=\text{P, As, Sb}$), respectively. From the atom specific phonon DOS of Fe_2ScP (Fig. 2(d)), we can see that higher energy optical phonon branches (~ 45 -55 meV) are contributed mainly from Sc atom. The considerable number of states for phonons due to the vibrations of lighter mass P atom is in the energy range ~ 30 -40 meV. The lower energy acoustic phonons in the range ~ 10 -22 meV are mainly due to the Sc and Fe atoms in the unit cell. The contributions to different branches in the phonon dispersion from the atoms in the unit cell of Fe_2ScAs can be understood from phonon PDOS in Fig. 2(e). The higher energy states of optical phonons in ~ 40 -50 meV are mainly contributed from lighter Sc atom in the formula unit. The major number of vibrational states lying in the intermediate energy region ~ 25 -30 meV can be attributed to Fe and As atoms. For Fe_2ScSb , TDOS and PDOS of phonon states are shown in Fig. 2(c) and (f), respectively. The heavier Sb atom is contributing considerably to the phonon states in ~ 10 -22 meV region. Like in the case of Fe_2ScAs , there is a small region in the neighborhood of 35 meV with no phonon states. The higher energy states of optical phonon states (~ 36 -43 meV) are primarily due to the Sc atoms (Fig. 2(f)). Fe atom contribution is mainly to phonons of energy ~ 22 -34 meV. The vibrational contribution of atoms X ($X=\text{P, As, Sb}$) in the unit cell of Fe_2ScX is shifting towards to the phonons of lower energy on crossing to Fe_2ScSb from Fe_2ScP . The increase in the atomic mass of X elements as well as increase in lattice constant mainly being the reason for this observed shift. But, in all the three cases the peaks in the higher energy range in DOS plots corresponding to three optical branches are substantially due

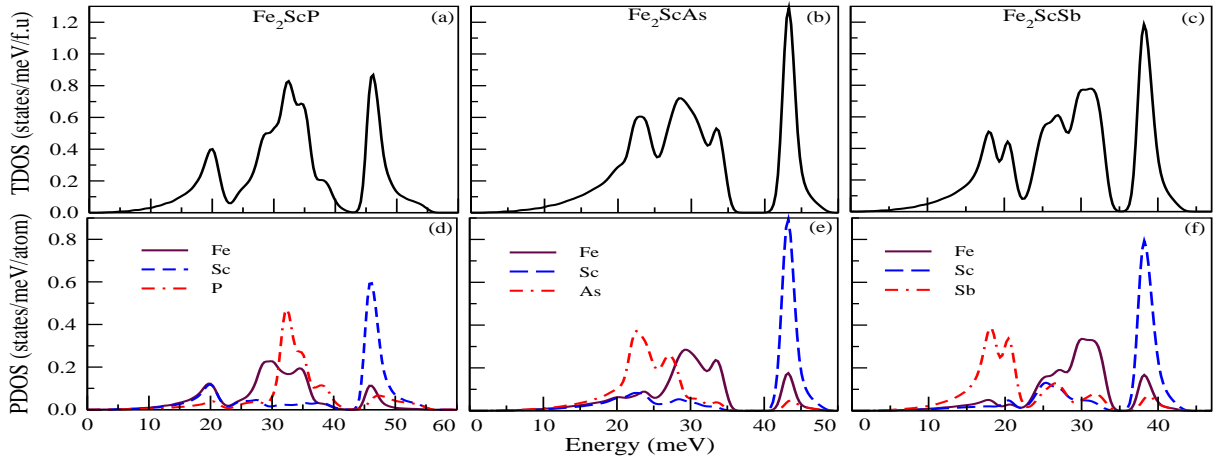


FIG. 2: Phonon TDOS and PDOS of Fe_2ScP , Fe_2ScAs and Fe_2ScSb .

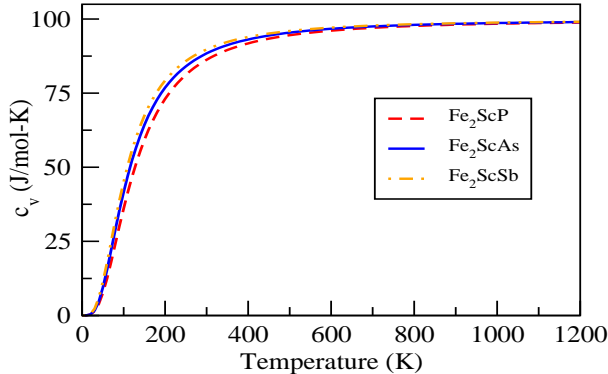


FIG. 3: Constant volume specific heat c_v curves of Fe_2ScP , Fe_2ScAs and Fe_2ScSb .

to vibrations of the Sc atom.

The lattice contributions to the constant volume specific heat c_v of Fe_2ScX compounds calculated under harmonic approximation are shown in Fig. 3. At higher temperatures (above 800 K) c_v curves are approaching the classical Dulong and Petit limit of ~ 100 J/mol-K for Fe_2ScX compounds. At any temperature, one can see that c_v values for $\text{Fe}_2\text{ScSb} > \text{Fe}_2\text{ScAs} > \text{Fe}_2\text{ScP}$

TABLE I: The indirect band gaps in eV obtained from mBJ, SCAN and PBEsol functionals.¹⁰

Functional	Fe_2ScP	Fe_2ScAs	Fe_2ScSb
mBJ	0.81	0.69	0.60
SCAN	0.31	0.14	0.06
PBEsol	0.30	0.09	-

compound. The lattice part of thermal conductivity is directly proportional to c_v and hence calculation of c_v is essential for an estimation of κ_{ph} of a TE material. From the nature of the curves, one can estimate that at higher temperatures the differences in κ_{ph} of Fe_2ScX compounds should be mainly due to group velocity and phonon relaxation time rather than due to c_v which are closer to each other in this case. Considering the definition of Debye frequency as a measure of the maximum phonon frequency and Debye temperature, Θ_D , to be the temperature above which all phonon modes begin to be excited²², the calculated values of Θ_D for Fe_2ScX (X=P, As, Sb) are ~ 637 K, ~ 556 K and ~ 498 K, respectively. The maximum phonon energy is decreasing from Fe_2ScP to Fe_2ScSb as mentioned earlier which is the reason for observed trend of Θ_D .

B. Electronic structure

The band gaps of semiconductors and insulators in KS-DFT calculations are generally underestimated. But, in a theoretical study or in prediction of new compounds with a band gap for thermoelectric applications, accurate calculation of band gap is essential since the number of carriers thermally excited varies exponentially with band gap. Also, in a DFT calculation, the curvature of bands at the band extrema and band features of electronic dispersion depends on the approximation used for the exchange-correlation part.¹¹ The transport coefficients calculated, depend on the effective mass and group velocity, which are derived from the band structure. Therefore, proper selection of XC functional for any DFT study of TE material is crucial. The question of which functional to choose was addressed in the work of Shamim *et al.*¹² as mentioned in the introduction which proposed that the combination of mBJ and SCAN (or PBEsol) functional would better explain the Seebeck coefficient. Thus, to calculate electronic band structure and dependent trans-

port properties, two functionals *viz.* SCAN and mBJ are used. The electronic bandstructure of Fe₂ScX (X=P, As, Sb) compounds are shown in Fig. 4(a)-(c), respectively. In the plots, the zero energy corresponds to the Fermi level, E_F , and is set to the middle of the gap. For each compound the indirect band gaps obtained from both functionals are listed in Table I. The indirect band gaps of Fe₂ScP and Fe₂ScAs obtained in the work of Sharma *et al.*¹⁰ are also included for comparison. Fe₂ScSb was predicted as semimetallic while former two compounds as semiconducting from PBEsol calculations in Ref. 10. As can be seen in Table I, the band gap values predicted by SCAN and PBEsol are closer to each other but, much lesser than that from mBJ. The band gaps of Fe₂ScP, Fe₂ScAs and Fe₂ScSb are 0.81, 0.69 and 0.60 eV, respectively as obtained from mBJ calculations. The mBJ is constructed to give accurate band gaps and the literatures show the good agreement between the experimental and mBJ calculated band gaps.^{11,23} Thus, band gaps predicted in this work could be useful numbers to experimentalists for comparison in case samples are prepared.

The band gap is reducing from Fe₂ScP to Fe₂ScSb by a value of approximately 0.1 eV in case of mBJ. Therefore, at a given temperature the number of electrons excited into the conduction band are relatively lower in Fe₂ScP compared to other two compounds with the relatively least number being in Fe₂ScSb. A band gap of mBJ ground state band structure has been introduced into the band structure of SCAN in such a way that conduction band minimum (CBM) at X -point and valence band maximum (VBM) at Γ -point from both functionals coincide. This representation of band structure from two functionals depicts (Fig. 4) the differences in the features of dispersion curves at different points along the k -path. The bands numbered 1 to 5 in Fig. 4 are denoted with symbols B1 to B5 in the description. The X atoms in the compound does not found to significantly affect the electronic states in the ~ -4 to -0.3 eV energy range of valence band region. Similarly, bands B1 and B2 in CB region are also slightly altered. This is discernible in the plots since the features of bands qualitatively does not show much difference in energy range mentioned.

In the plots the valence band maximum (VBM) is at Γ -point and CBM is at X -point giving indirect band gaps. In all three compounds, the VBM is triply degenerate at Γ -point. Fe₂ScX compounds possess a band B2 which is almost flat along the Γ - X direction and is dispersive in the direction Γ - L - W . The bands B1 and B2 are degenerate at Γ -point and continues to show degeneracy till L -point. The bands B1 and B2 start at the same energy at W but along the W - Γ and Γ - X directions, the bands of SCAN are elevated in energy relative to the mBJ bands. The three valence bands of SCAN starting from Γ and along the directions L - W and X - W - K are higher in energy relative to mBJ bands. In other words, in the VB region nearer to E_F , SCAN bands are narrower compared to mBJ bands (B3-B5) which implies density of states should be higher near E_F in electronic structure

calculated from SCAN. The CBM at Γ -point is doubly degenerate, but the bands 1 and 2 obtained from mBJ are relatively more narrower compared to the bands of SCAN. This implies the density of states in the CB region near E_F is more in mBJ approximated electronic ground state.

The relatively small number of electrons excited into the conduction band decide the transport behavior in a semiconductor.²² Since, the excited carriers are found almost in the neighborhood of the CB minima or VB maxima, for the three compounds the band extrema are approximated with a parabola to calculate the effective mass. Under the parabolic approximation, effective mass is inversely proportional to the curvature of the parabolic band. Thus, the effective mass values of carriers in a band indicates the curvature of the band. The Seebeck coefficient (S) is directly proportional to the effective mass of charge carriers in the material according to the equation⁴,

$$S = (8\pi^2 k_B^2 / 3eh^2) m^* T (\pi / 3n)^{2/3}. \quad (2)$$

In the above relation, h is Planck's constant, k_B is Boltzmann constant, e is electronic charge and n is carrier concentration, respectively.

The direct band gap from mBJ in these materials are 0.85, 0.72 and 0.62 eV, respectively (Fig. 4). These values of energy gap are much close to the indirect band gaps of mBJ listed in Table I and hence there is finite probability that electron transition takes place between these points too. In order to quantify the curvature of bands from SCAN, the parabola were fitted at band extrema according to the free electron energy equation $E = \frac{\hbar^2 k^2}{2m_e m^*}$, where m_e is rest mass of electron and m^* effective mass in terms of mass of electron. The bands numbered 1 to 5 (labeled B1 to B5 in Table II) in Fig. 4 which significantly participate in the transport are fitted with parabola in the vicinity of CB minima at Γ and X -points and VB maximum at Γ -point for SCAN functional. The obtained values of effective mass along different directions for Fe₂ScX (X=P, As, Sb) for SCAN bands are listed in Table II. The notation, for instance, $\Gamma - \Gamma L$ denotes the effective mass calculated at Γ -point along Γ to L direction.

The effective mass values in Table II clearly highlight the large m^* for band B2 in all three compounds. Along $X - W$ direction m^* are 39.91, 36.67 and 37.69 for three compounds, respectively. For the same band along Γ - X direction carriers have m^* greater than along $X - W$ direction. In Fe₂ScP, effective mass m^* of the bands B1-B4 is 0.26 and B5 is 0.22, respectively along Γ - L directions. Along the Γ - X direction m^* of bands B1, B5, and B3 and B4 are 0.13, 0.14, 0.43 and 0.42, respectively. As can be seen from the table, the band B2 has very large value of effective mass (m^*) along $\Gamma - X$ and $X - \Gamma$ directions and can be called heavy band in Fe₂ScX. From Fig. 4 one can observe that at CBM and VBM at the Γ -point, the curvature of mBJ bands are lesser compared to that of SCAN bands. This implies that effective mass if estimated from mBJ should be higher for these compounds.

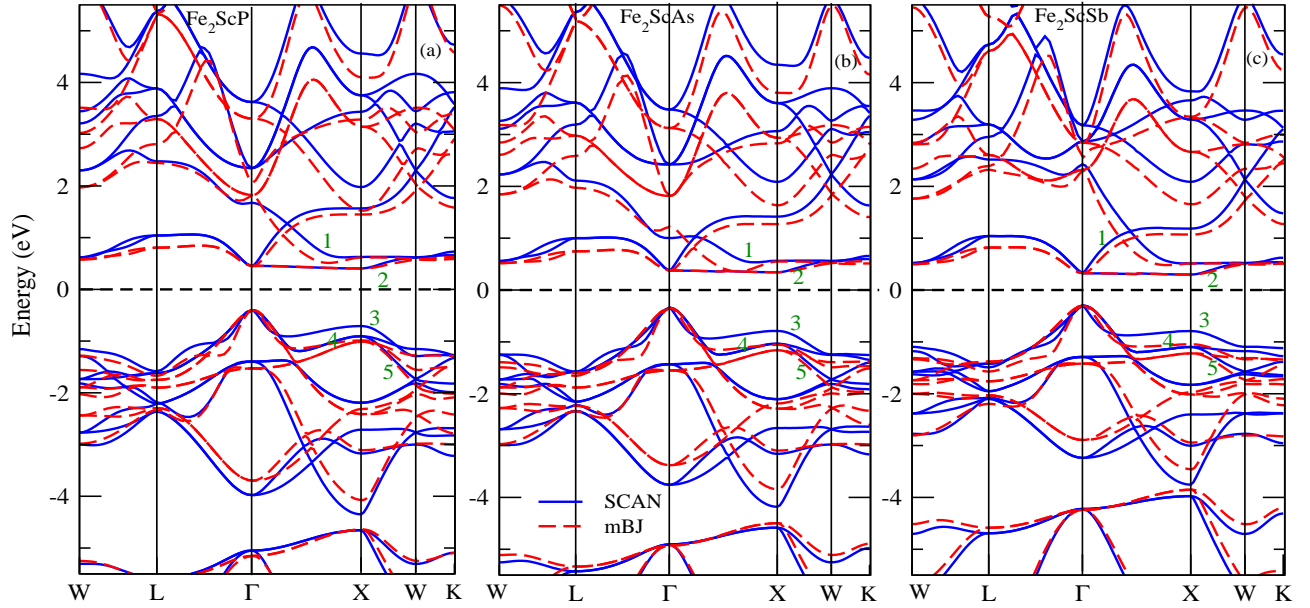


FIG. 4: Electronic band structures of Fe_2ScP , Fe_2ScAs and Fe_2ScSb . The blue (solid) lines represent bands from SCAN and red (dashed) lines are from mBJ.

TABLE II: Effective mass (m^*) of charge carriers calculated for Fe_2ScX (X=P, As, Sb compound at Γ and X points respectively, in various bands from SCAN.

	Fe_2ScP				Fe_2ScAs				Fe_2ScSb			
	Γ - Γ L	Γ - Γ X	X-X Γ	X-XW	Γ - Γ L	Γ - Γ X	X-X Γ	X-XW	Γ - Γ L	Γ - Γ X	X-X Γ	X-XW
B1	0.26	0.13			0.19	0.10			0.16	0.09		
B2	0.26	20.56	39.91	1.36	0.19	46.79	36.67	1.46	0.16	50.25	37.69	1.25
B3	0.26	0.43			0.21	0.41			0.22	0.45		
B4	0.26	0.42			0.19	0.41			0.16	0.45		
B5	0.22	0.14			0.19	0.10			0.16	0.09		

In the work of Kim *et al.*²³ for III-V semiconductors effective mass values were estimated using mBJ and found that mBJ effective masses are overestimated with respect to experimental data by ~ 30 -50 %. Thus, one may predict that effective mass calculated for SCAN should be nearer to experimental value since these band features also explained the Seebeck coefficient of Fe_2VAl in Ref. 12. For a given compound, along the $\Gamma - L$ direction the bands B1 to B5 have nearly same curvature. While, along $\Gamma - L$ direction, B3 and B4 bands are of similar curvature which is justified by the m^* values in the table.

C. Thermoelectric properties

The thermoelectric parameters Seebeck coefficient S , electrical conductivity per relaxation time σ/τ and power factor per relaxation time $S^2\sigma/\tau$ (PF), are calculated for Fe_2ScX compounds under semiclassical transport theory. In order to calculate TE properties, the band structure from SCAN functional and band gap obtained from the

mBJ have been used. In Fig. 5(a)-(c), for three compounds the variation S with the shifts in chemical potential (μ) are presented at 300 K. The dashed line normal to μ axis indicates chemical potential for the intrinsic compounds at 0 K. The positive and negative values of μ in plots correspond to electron and hole doping, respectively. At the temperature of 300 K, S vs. μ curve cuts the $\mu=0$ line, for Fe_2ScP , at $\sim -1134 \mu\text{VK}^{-1}$ and for Fe_2ScAs and Fe_2ScSb at ~ -1068 and $\sim -963 \mu\text{VK}^{-1}$, respectively. This indicates intrinsic Fe_2ScX at 300 K will show negative S values which is attributed mainly due to presence of flat conduction band in these compounds. The values of extrema in the S curves are reducing from Fe_2ScP to Fe_2ScSb which implies in Fe_2ScP maximum S can be obtained either by electron or hole doping.

The maximum value of S (at 300 K) for the three compounds are ~ -1421 , ~ -1230 and $\sim -1080 \mu\text{VK}^{-1}$ in the order, for shift in μ of ~ 34 , ~ 23 and ~ 24 meV, respectively. While, the maximum positive S values that can be attained by hole doping is relatively lesser compared to electron doping and also requires more doping (Fig.

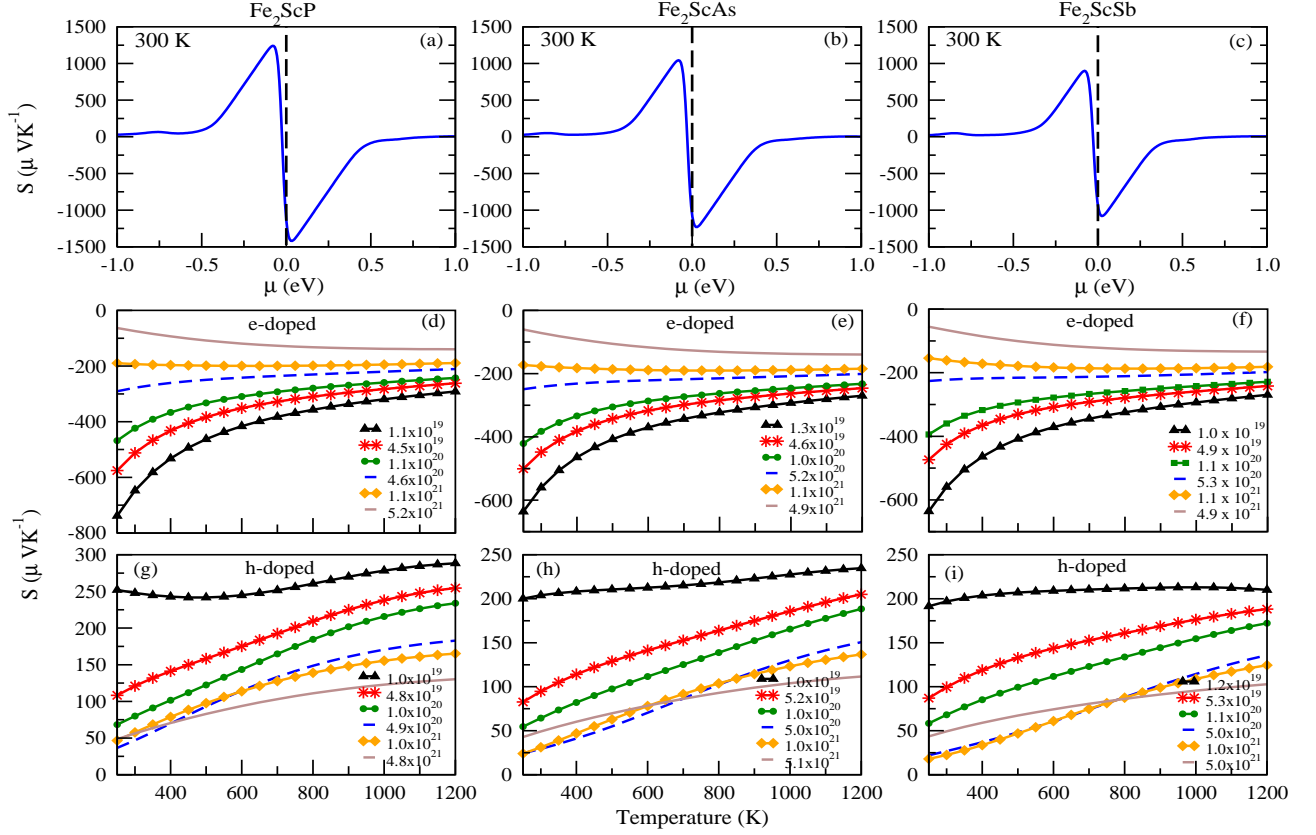


FIG. 5: Seebeck Coefficient (S) vs. chemical potential (μ) plots (Fig. 5(a)-(c)) and S as a function of temperature (T) for electron doping (Fig. 5(d)-(f)) and hole doping (Fig. 5(g)-(i)). Each of three vertical panel in the figure shows the plots for Fe_2ScP , Fe_2ScAs and Fe_2ScSb , respectively.

5(a)-(c), large shift in μ towards negative side) to get high S value. At a given temperature, the S is inversely proportional to carrier concentration (n) and directly proportional to m^* . The band gap of Fe_2ScP is 0.81 eV and is the highest in the family of Fe_2ScX (Table I) making n to be smaller compared to other compounds at a given temperature. This explains the reason for the observed higher S in Fig. 5(a) for Fe_2ScP compared to other two compounds. We compare the S vs. μ curves with the work of Sharma *et al.*¹⁰ wherein PBEsol functional was used. We observe that the extrema of S values calculated as a function of μ at 300 K are very much lower compared to that of our work. The maximum value of S in Ref. 10 for undoped compounds (at $\mu=0$) was -770, -386, -192 μVK^{-1} for Fe_2ScP , Fe_2ScAs and Fe_2ScSb , respectively. This can be mainly due to the lower band gap predicted by PBEsol (Table I) for Fe_2ScX compounds.

In order to find out the proper carrier concentration that would yield S and σ/τ values which maximize the PF, we have doped Fe_2ScX compounds with electrons and holes in the range $\sim 1 \times 10^{19}$ to $\sim 5 \times 10^{21}$ cm^{-3} . For

the three compounds S , σ/τ and PF values are calculated for various dopings in the temperature range 250-1200 K. Seebeck coefficient values for electron doped compounds are shown in Fig.5 (d)-(f). For Fe_2ScX , values of S are decreasing continuously with the increase in the temperature for a given electron doping from $\sim 1 \times 10^{19}$ cm^{-3} to $\sim 1 \times 10^{20}$ cm^{-3} . For $\sim 5 \times 10^{20}$ cm^{-3} of doping, the range of S (max. S -min. S) for temperature range under study is reduced. For $\sim 1 \times 10^{21}$ cm^{-3} of doping the S is not varying substantially with temperature. But, slow increasing nature of S is observed for $\sim 5 \times 10^{21}$ cm^{-3} . This is the general trend of S observed in case of electron doping. Also, with increase in the electron doping S curves are shifting towards lower values since S varies inversely with carrier concentration as given by Eq. (2). The maximum values of S are ~ 743 , ~ 645 , ~ 637 μVK^{-1} for $\sim 1 \times 10^{19}$ cm^{-3} electron doping for Fe_2ScX compounds, respectively at 250 K. At any temperature lower doping of $\sim 1 \times 10^{19}$ cm^{-3} has higher S value. In Ref. 10, nature of the S curves for $\sim 1 \times 10^{19}$ - $\sim 1 \times 10^{21}$ cm^{-3} of doping are different which can be due the lower band gaps consid-

ered compared to present work. The maximum S values at $\sim 1 \times 10^{19} \text{ cm}^{-3}$ doping are ~ 500 , ~ 400 and $\sim 25 \mu\text{VK}^{-1}$ for Fe_2ScX , respectively.

The nature of S curves for different hole dopings are shown in Fig. 5(g)-(i) for three compounds. The maximum S is obtained for doping of $\sim 1 \times 10^{19} \text{ cm}^{-3}$ in the temperature range considered and the increment in S with the increase in the temperature is less compared to higher dopings. For $\sim 5 \times 10^{19} \sim 5 \times 10^{21} \text{ cm}^{-3}$ range, S is increasing with nature of S almost linear in 250-1200 K. But, Seebeck coefficients for dopings of $\sim 1 \times 10^{21} \text{ cm}^{-3}$ and above are crossing lower doping curves at higher temperatures. In Ref. 10, S curves for hole doping does not show linear increase behavior as in this work, instead there are peaks in the S curves. The reason for the observed differences may be due to the large band gap considered in this work. Comparing the S , for hole and electron doped case, one can observe that from Fig. 5, for a given doping electron doping gives larger S for Fe_2ScX .

The Figure 6 shows the σ/τ and PF plots for different carrier concentrations as a function of temperature. The electron and hole doping values considered for both σ/τ and PF are shown only in the respective PF plots, represented in same colors (or symbols). The highlighting feature of σ/τ plots (Fig. 6(a)-(f)) is that, for any doping values σ/τ curves are nearly linearly increasing from 250 to 1200 K for all compounds. For doping of $\sim 1 \times 10^{19} \sim 1 \times 10^{20} \text{ cm}^{-3}$, σ/τ curves are close to each other for both electron and hole doping. For higher dopings σ/τ curves are shifting towards higher values. The highest σ/τ is obtained for doping concentration of $\sim 5 \times 10^{21} \text{ cm}^{-3}$ of both electron and hole type. From $\sim 5 \times 10^{20}$ to $\sim 5 \times 10^{21} \text{ cm}^{-3}$, the obtained value of σ/τ , for a given doping concentration is higher for hole type doping compared to electron type. This can be understood as because of the lesser effective mass of holes in valence bands (B3-B5)(Table II) compared to that of electrons with high effective mass in band B2. Since, the charge carrier with higher effective mass has lower mobility and electrical conductivity in semiconductors is related to mobility as, $\sigma = ne\mu_c$, where μ_c is mobility of charge carriers, higher electrical conductivity of holes is expected in these compounds.

The $S^2\sigma/\tau$ (PF) plots for Fe_2ScX are presented in Fig. 6 (g)-(l) for electron and hole doping in $10^{14} \mu\text{WK}^{-2} \text{cm}^{-1} \text{s}^{-1}$ ($= 1$ PF unit, PFU). For electron doped cases, the PF curves are shifted to higher values with the increased doping concentration except for doping of $\sim 5 \times 10^{21} \text{ cm}^{-3}$. For a given doping, the PF is increasing with temperature from 250 to 1200 K. For temperatures of practical applications, for instance, in automobiles where temperature of heat source, to install TEG is considered as 800 K²⁴, PF values at these temperatures are, ~ 121 , ~ 125 and ~ 131 PFU, for doping of $\sim 1 \times 10^{21} \text{ cm}^{-3}$ for Fe_2ScP , Fe_2ScAs , and Fe_2ScSb , respectively. Thus, for Fe_2ScX compounds, to get a high PF from electron doping, $\sim 1 \times 10^{21} \text{ cm}^{-3}$ can be consid-

ered as optimal doping concentration in the doping range considered.

For hole doped case also an increasing trend in PF with temperature is observed in Fig. 6 (j)-(l). For doping range $\sim 1 \times 10^{19} \sim 1 \times 10^{20} \text{ cm}^{-3}$, the PF values are close to each other. At any temperature, for the hole doping of $\sim 5 \times 10^{21} \text{ cm}^{-3}$ highest PF is obtained for these compounds. At 800 K, the values of PF for $\sim 5 \times 10^{21} \text{ cm}^{-3}$ dopings are, ~ 118 , ~ 83 and ~ 63 PFU for Fe_2ScP , Fe_2ScAs , and Fe_2ScSb , respectively. From Fig. 6 (j)-(l) we can observe that PF values for a given doping is decreasing from Fe_2ScP to Fe_2ScSb . The power factor curves in the work of Ref. 10 shows gradual increasing behavior for the carrier concentration of $\sim 1 \times 10^{17}$ to $\sim 1 \times 10^{19} \text{ cm}^{-3}$. But, for doping of $\sim 1 \times 10^{20}$ to $\sim 1 \times 10^{21} \text{ cm}^{-3}$, there are peaks in the PF curves. The maximum PF is obtained for a doping of $\sim 5 \times 10^{21} \text{ cm}^{-3}$ in all three compounds. The maximum values of PF obtained for p-type doping is ~ 90 -24 PFU and for n-type doping is ~ 85 -54 PFU from Fe_2ScP to Fe_2ScSb compound in Ref. 10. The values of maximum PFs obtained by using PBESol functional in the work of Ref. 10 are lesser compared to the present work. The band gaps obtained by PBESol are lesser compared to mBJ as can be seen in Table I, may be the reason for the observed differences in PF values calculated in two works. From the nature of the PF curves (Fig. 6 (g)-(l)), which are showing increasing behaviour with temperature, we can propose these materials for high temperature thermoelectric applications.

Electronic thermal conductivity per relaxation time (κ_e/τ) of Fe_2ScX compounds for electron and hole dopings considered in this study are shown in Fig. 7 (a)-(c) and (d)-(f), respectively. For three compounds, κ_e/τ curves are showing increasing trend with temperature. For optimal doping cases giving the highest PFs *viz.* $\sim 1 \times 10^{21} \text{ cm}^{-3}$ of electron doping, κ_e/τ is increasing from first to last compound while, for hole doping of $\sim 5 \times 10^{21} \text{ cm}^{-3}$ reverse trend is observed. At 800 K, κ_e/τ values for electron doping of $\sim 1 \times 10^{21} \text{ cm}^{-3}$ which yields the highest PF are 0.13, 0.14 and 0.15 $10^{16} \text{ Wm}^{-1} \text{K}^{-1} \text{s}^{-1}$ for Fe_2ScX compounds, respectively.

Calculation of κ of TE material is important to fully evaluate it for TE application. But, calculation of κ_{ph} is a difficult and computationally demanding task²⁵. Therefore, any simple method predicting fairly good value of κ_{ph} is of much help. Here for a quantitative estimation of κ_{ph} in Fe_2ScX compounds we resort to a simple method which turns out to provide reasonably good estimation of κ_{ph} . The relation for κ_{ph} is given by²²,

$$\kappa_{ph} = \frac{1}{3} c_v c^2 \tau_{ph}, \quad (3)$$

where c_v is constant volume specific heat per unit volume, c is phonon phase velocity in linear dispersion and τ_{ph} is phonon relaxation time.

Now, to calculate κ_{ph} from Eq. 3, the values of c_v , c and τ_{ph} are needed. The specific heat, c_v is obtained as function of temperature from the phonon calculations.

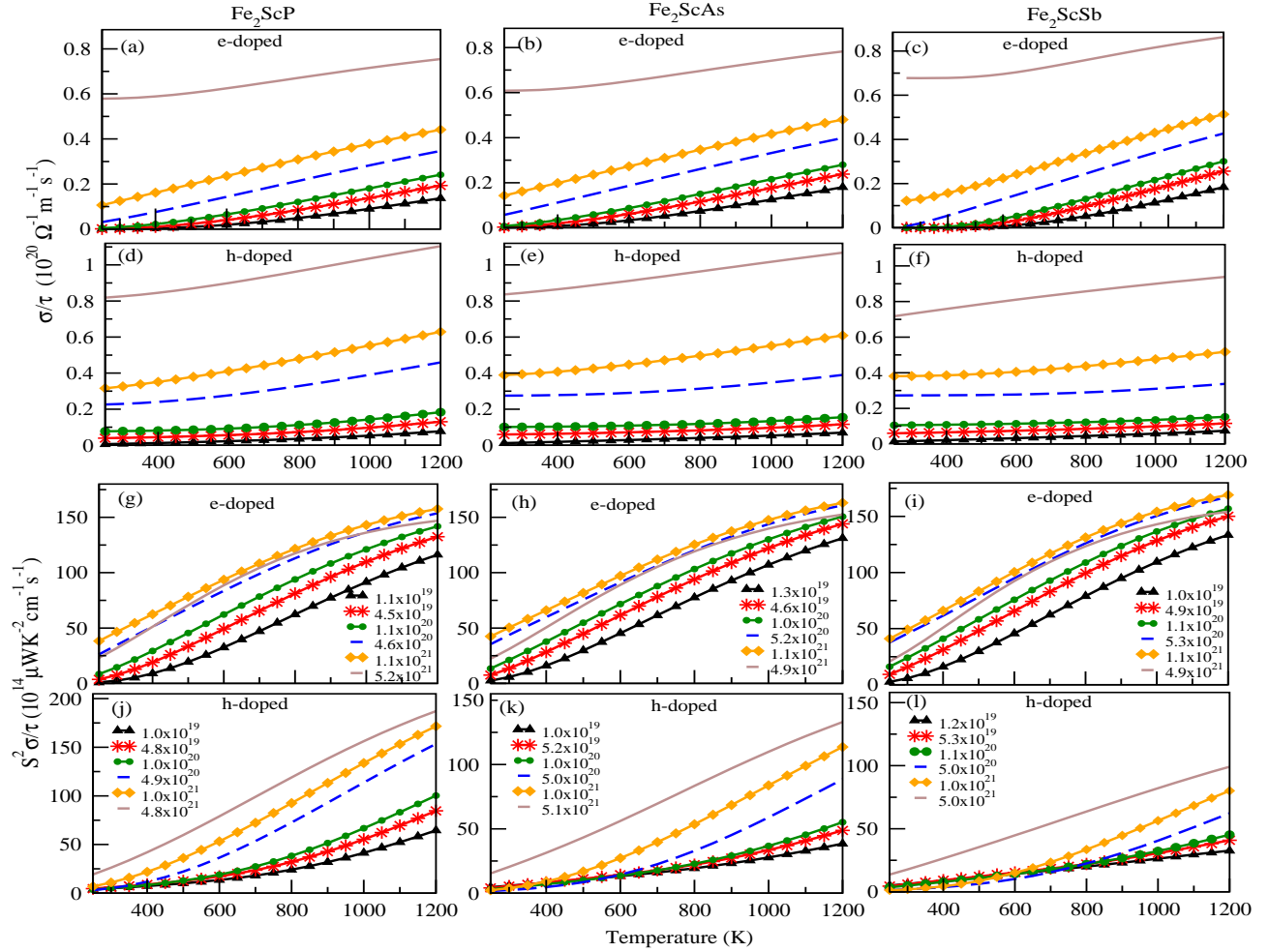


FIG. 6: Electrical conductivity per relaxation time (σ/τ) and power factor per relaxation time ($S^2\sigma/\tau$) as a function of temperature (T) for electron doping (Fig. 6(a)-(c) and (g)-(i)) and hole doping (Fig. 6(d)-(f) and (j)-(l)) for Fe_2ScP , Fe_2ScAs and Fe_2ScSb , respectively.

To calculate c , three acoustic branches are approximated with linear dispersion, by fitting with straight line in the neighborhood of Γ ($\mathbf{k} = \mathbf{0}$) of the calculated phonon dispersions. Then c is calculated as $c = \omega/k$, the slope of the linear dispersion. To find out c , acoustic branches in the Γ - W and Γ - L directions are considered. Values of c of three acoustic branches in two directions are averaged, which we denote by c_{avg} and used to estimate κ_{ph} instead of c in Eq. 3. Table III shows the values of c calculated for three acoustic branches in two directions and c_{avg} values for Fe_2ScX , Fe_2VAI and Fe_2TiSn compounds. The branch notations followed are shown in the inset of Fig. 1 (b).

The Table III shows that the c of phonons of three acoustic branches in Γ - L directions are reducing from Fe_2ScP to Fe_2ScSb . In Γ - W direction, similar trend in c is noted for branch S2 and S3 (which are degenerate), except for S1 in which opposite trend is observed. In Γ - L direction, branches S1 and S2 are degenerate and have value of c , 102.4, 86.5 and 78.5 $\text{THz} \cdot \text{Bohr}$ for Fe_2ScX ,

respectively. The c_{avg} for Fe_2ScX are 112.2, 99.2, and 91.0 $\text{THz} \cdot \text{Bohr}$, respectively. The observed trend is due to reduction in phonon frequencies on going from first to last compound. In both directions considered, c values of phonons in Fe_2VAI is greater than that in Fe_2TiSn for all branches. The calculated c_{avg} are 116.6 and 107.1 $\text{THz} \cdot \text{Bohr}$ for Fe_2VAI and Fe_2TiSn , respectively. The phonon c_{avg} of Fe_2ScX compounds are lesser compared to Fe_2VAI and Fe_2TiSn except, for Fe_2ScP with c_{avg} of 112.2 $\text{THz} \cdot \text{Bohr}$.

Once, the quantities c_v and c are known, τ_{ph} needs to be found out which is the computationally more difficult part. At this step, to estimate the value of τ_{ph} , we considered Fe_2VAI and later the τ_{ph} is benchmarked using Fe_2TiSn compound. For the estimation, c_v values are taken from our previous work¹⁹ and c_{avg} (and c) used are calculated and tabulated in Table III. Using the experimental κ of Fe_2VAI ²⁶ at 300 K of $\sim 25 \text{ W m}^{-1} \text{ K}^{-1}$, the τ_{ph} estimated, is $\sim 5 \times 10^{-13} \text{ s}$. The calculated value of κ_{ph} for Fe_2TiSn using the estimated τ_{ph} at the same temper-

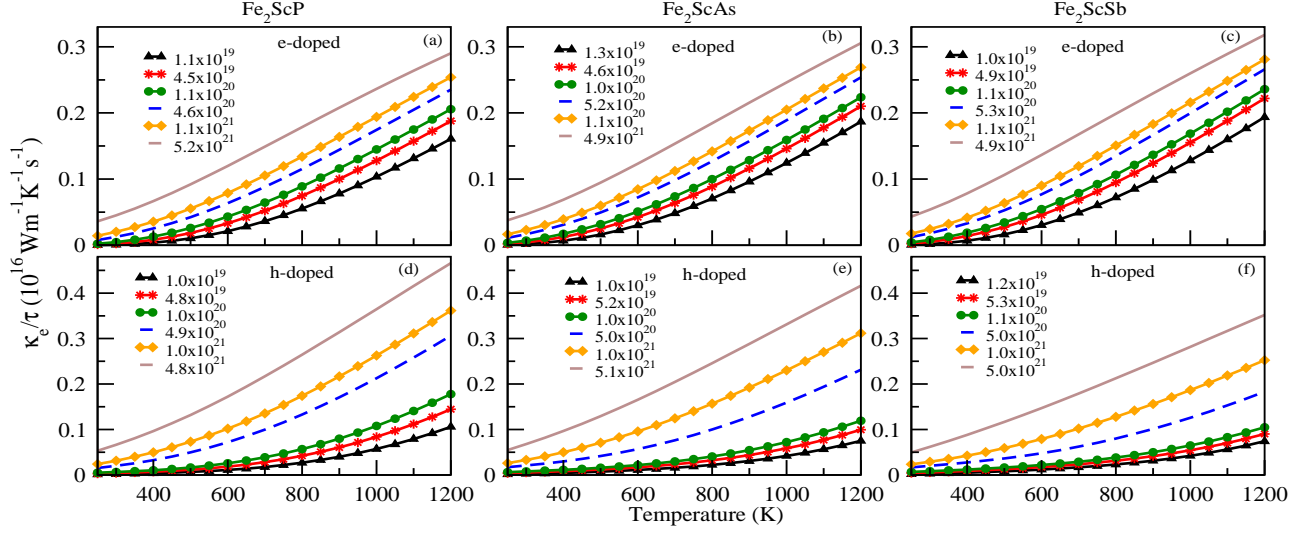


FIG. 7: Electronic thermal conductivity per relaxation time (κ_e/τ) as a function of temperature (T) for electron doping (Fig. 7(a)-(c)) and hole doping (Fig. 7 (d)-(f)) for Fe_2ScP , Fe_2ScAs and Fe_2ScSb , respectively.

ature is $\sim 14.8 \text{ Wm}^{-1}\text{K}^{-1}$. This value is close to the experimental κ value of Leu *et al.*²⁷ ($\sim 7 \text{ Wm}^{-1}\text{K}^{-1}$) at 300 K. This suggests that the τ_{ph} estimated by this method can predict reasonably accurate values of κ_{ph} for other three compounds using such a simple approach. It is important to note here that, Fe_2VAl , Fe_2TiSn and Fe_2ScX compounds have same crystal structure and belong to the same class of compounds with similar phonon dispersions which led us to select the former two compounds in the estimation. With the calculated τ_{ph} of $5 \times 10^{-13} \text{ s}$ and using c_{avg} and c_v values, the estimated κ_{ph} at 300 K for three compounds are 18.2, 13.6 and $10.3 \text{ Wm}^{-1}\text{K}^{-1}$, respectively. The κ_{ph} is reducing from Fe_2ScP to Fe_2ScSb , which may be mainly due to the larger sized and heavier mass elements in the latter compounds.

The assessment of TE applicability of Fe_2ScX Heusler compounds is done by calculating temperature dependent ZT in 300-1200 K range. For the calculation of ZT from Eq. 1, the estimated κ_{ph} at 300 K of the pure compounds are used for all temperatures, which is generally expected to reduce at higher temperatures. Constant electron relaxation time τ of $1 \times 10^{-14} \text{ s}$ is used²² in the estimation of $S^2\sigma$ and κ_e . The temperature dependent ZT values of Fe_2ScX compounds are calculated for the highest PF yielding optimal electron (n-type) doping of $\sim 1 \times 10^{21} \text{ cm}^{-3}$ and hole (p-type) doping of $\sim 5 \times 10^{21} \text{ cm}^{-3}$, out of the doping range considered in this study. The obtained ZT for doped Fe_2ScX compounds are presented in Fig. 8. The ZT values suggest that Fe_2ScX compounds could be promising materials for TE applications with ZT showing the increasing nature with temperature.

From the figure we can see that for electron doping shown, Fe_2ScSb has the highest ZT while, for hole doping Fe_2ScP shows the highest ZT among the family. The highest ZT is obtained from Fe_2ScSb , which in 300-500 K is 0.11-0.25, in the mid-temperature range of 500-900 K is 0.25-0.45 and in high temperature range 900-1200 K is 0.45-0.52. The ZT values obtained from the hole doping of $\sim 5 \times 10^{21} \text{ cm}^{-3}$ for these compounds are lower compared to electron doping. The n-type Fe_2ScP has ZT in the range 0.07 to 0.43, while p-type Fe_2ScP has 0.03-0.34 which is the highest among p-type Fe_2ScX compounds. The doped Fe_2ScAs is showing intermediate ZT among the optimal doped Fe_2ScX compounds. The ZT range for n-type and p-type Fe_2ScAs are 0.09-0.48 and 0.03-0.28 in 300-1200 K, respectively. For last compound in the family, n-type Fe_2ScSb , the highest ZT is observed in the range of 0.11-0.52. In case of it's p-type counterpart of $\sim 5 \times 10^{21} \text{ cm}^{-3}$ doped, ZT at 300 K is 0.03 and it is reaching 0.26 at 1200 K. Higher ZT values are observed in the high temperature region for both type of doping, which hints at the possible applicability in high temperature power generation. The 900-1200 K range ZT for $\sim 1 \times 10^{21} \text{ cm}^{-3}$ doping of Fe_2ScX compounds are, 0.34-0.43, 0.40-0.48 and 0.45-0.52, respectively. For the hole doping of $\sim 5 \times 10^{21} \text{ cm}^{-3}$, the ZT values in the same temperature range are 0.25-0.34, 0.20-0.28 and 0.18-0.26, respectively.

The higher ZT observed at temperatures $> 900 \text{ K}$, indicates that for the high temperature TE power generation, doped Fe_2ScX full-Heuslers could be one of the suitable candidates. Currently, doped Si-Ge alloys are one of TE materials in use for power generation in high tempera-

TABLE III: Phase velocity (c) of three acoustic branches (S1-S3) in Γ - W and Γ - L directions and average of phase velocities, c_{avg} , for Fe_2ScX ($X=\text{P, As, Sb}$), Fe_2VAl and Fe_2TiSn compounds in $\text{THz} \cdot \text{Bohr}$

	Fe_2ScP		Fe_2ScAs		Fe_2ScSb		Fe_2VAl		Fe_2TiSn	
	Γ - W	Γ - L	Γ - W	Γ - L	Γ - W	Γ - L	Γ - W	Γ - L	Γ - W	Γ - L
S1	69.9	102.4	71.0	86.5	73.4	78.5	96.7	101.4	80.1	93.1
S2	95.5	102.4	84.4	86.5	78.1	78.5	101.4	101.4	90.4	93.1
S3	161.9	141.0	138.7	128.3	120.6	117.1	151.1	147.8	146.2	139.9
c_{avg}	112.2		99.2		91.0		116.6		107.1	

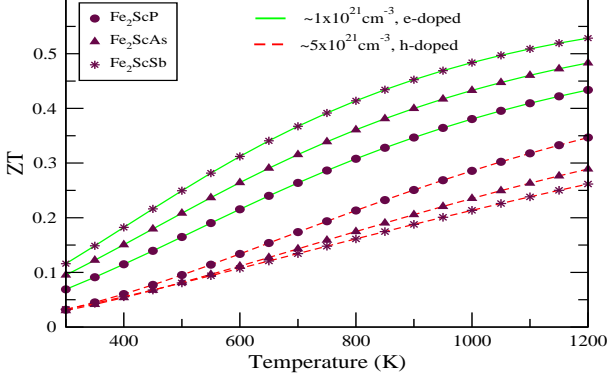


FIG. 8: Temperature dependent ZT plot of Fe_2ScX ($X=\text{P, As, Sb}$) compounds for electron doping of $\sim 1 \times 10^{21} \text{ cm}^{-3}$ shown in solid (green) lines and hole doping of $\sim 5 \times 10^{21} \text{ cm}^{-3}$ in dashed (red) lines.

ture region with ZT ranges in 673-1273 K of ~ 0.5 - 0.8 and ~ 0.4 - 0.6 for n-type and p-type Si-Ge, respectively⁴. The simultaneous increase in thermopower and electrical conductivity with moderate decrease in thermal conductivity was observed in the work of Makongo *et al.*²⁸ leading to ~ 2.5 times ZT enhancement for the bulk nanostructured (Zr,Hf)NiSn half-Heusler alloys. In the TE research, with the considerable interest in enhancement of ZT by complex nanostructuring^{4,29}, we anticipate that Fe_2ScX family of full-Heusler could be worth considering next to Si-Ge alloys. Also, the ZT plot, hints that, with both electron and hole doped compounds showing good ZT number, they can be used as n-type and p-type thermoelements in constructing TEGs. Therefore, an attempt by experimental community to synthesize and study the TE properties are highly desired.

IV. CONCLUSIONS

In the present work, electronic structure and dependent thermoelectric coefficients of Fe_2ScX ($X=\text{P, As, Sb}$) compounds are studied using two functionals *viz.* SCAN and mBJ. The differences in the features of the electronic bands obtained from mBJ and SCAN are brought out by

comparison. The effective mass values are calculated at the bands extrema of SCAN. The indirect band gaps for Fe_2ScP , Fe_2ScAs and Fe_2ScSb , obtained from mBJ are 0.81, 0.69 and 0.60 eV, respectively. S , σ/τ , PF and κ_e/τ are calculated for various values of electron and hole doping by introducing band gaps from mBJ into band structures of SCAN under semiclassical transport equations. The PF obtained at the temperature of 800 K for electron doping of $\sim 1 \times 10^{21} \text{ cm}^{-3}$ are ~ 121 , ~ 125 and $\sim 131 \text{ } 10^{14} \mu\text{WK}^{-2} \text{ cm}^{-1} \text{ s}^{-1}$ for Fe_2ScX where $X=\text{P, As, Sb}$, respectively. While, at the same temperature, highest PF values is obtained for hole doping of $\sim 5 \times 10^{21} \text{ cm}^{-3}$ are ~ 118 , ~ 83 and $\sim 63 \text{ } 10^{14} \mu\text{WK}^{-2} \text{ cm}^{-1} \text{ s}^{-1}$ for Fe_2ScX , respectively. The phonon dispersion and density of states are calculated for the three compounds which supported the structural stability. The calculated lattice contribution to c_v shows at any temperature c_v are in order $\text{Fe}_2\text{ScSb} > \text{Fe}_2\text{ScAs} > \text{Fe}_2\text{ScP}$. The maximum phonon energy (or frequency) for Fe_2ScX are ~ 55 , ~ 48 and ~ 43 meV, respectively. The Debye temperatures are calculated for three compounds which are ~ 637 K, ~ 556 K and ~ 498 K, respectively. Based on the calculation of slopes of acoustic branches in the linear region and estimated τ_{ph} , κ_{ph} of Fe_2ScX compounds at 300 K are estimated. The κ_{ph} for three compounds are 18.2, 13.6 and $10.3 \text{ Wm}^{-1} \text{ K}^{-1}$, respectively. In the temperature range 900-1200 K, the ZT values are 0.25-0.34, for the hole doping of $\sim 5 \times 10^{21} \text{ cm}^{-3}$ are 0.20-0.28 and 0.18-0.26, respectively. In the same temperature range, ZT for $\sim 1 \times 10^{21} \text{ cm}^{-3}$ doping are 0.34-0.43, 0.40-0.48 and 0.45-0.52, respectively. Our work suggests that Fe_2ScX compounds could be worth considering for high temperature TE applications with both n-type and p-type compounds showing good ZT values.

V. ACKNOWLEDGEMENTS

The authors thank Science and Engineering Research Board (SERB), Department of Science and Technology, Government of India for funding this work. This work is funded under the SERB project sanction order No. EMR/2016/001511.

VI. REFERENCES

-
- * Electronic mail: shastri1992@gmail.com
† Electronic mail: sudhir@iitmandi.ac.in
- ¹ P. Gorai, V. Stevanović, and E. S. Toberer, *Nat. Rev. Mater.* **2**, 17053 (2017).
 - ² T. M. Tritt and M. Subramanian, *MRS bulletin* **31**, 188 (2006).
 - ³ J. Yang, L. Xi, W. Qiu, L. Wu, X. Shi, L. Chen, J. Yang, W. Zhang, C. Uher, and D. J. Singh, *NPJ Comput. Mater.* **2**, 15015 (2016).
 - ⁴ G. J. Snyder and E. S. Toberer, *Nat. Mater.* **7**, 105 (2008).
 - ⁵ G. Mahan and J. Sofo, *Proc. Nat. Acad. Sci.* **93**, 7436 (1996).
 - ⁶ S. Sharma and S. K. Pandey, *J. Phys.: Condens. Matter* **26**, 215501 (2014).
 - ⁷ S. Yabuuchi, M. Okamoto, A. Nishide, Y. Kurosaki, and J. Hayakawa, *Appl. Phys. Express* **6**, 025504 (2013).
 - ⁸ J. Barth, G. H. Fecher, B. Balke, T. Graf, A. Shkabko, A. Weidenkaff, P. Klaer, M. Kallmayer, H.-J. Elmers, H. Yoshikawa, *et al.*, *Phil. Trans. R. Soc. A* **369**, 3588 (2011).
 - ⁹ J. Barth, G. H. Fecher, B. Balke, S. Ouardi, T. Graf, C. Felser, A. Shkabko, A. Weidenkaff, P. Klaer, H. J. Elmers, *et al.*, *Phys. Rev. B* **81**, 064404 (2010).
 - ¹⁰ S. Sharma and S. K. Pandey, *J. Phys. D: Appl. Phys.* **47**, 445303 (2014).
 - ¹¹ S. S. Shastri and S. K. Pandey, *Comput. Mater. Science* **143**, 316 (2018).
 - ¹² S. Sk, P. Devi, S. Singh, and S. K. Pandey, *Mater. Res. Express* **6**, 026302 (2018).
 - ¹³ P. Blaha, K. Schwarz, G. K. H. Madsen, D. Kvasnicka, and J. Luitz, An augmented plane wave+ local orbitals program for calculating crystal properties (2001).
 - ¹⁴ F. Tran and P. Blaha, *Phys. Rev. Lett.* **102**, 226401 (2009).
 - ¹⁵ J. Sun, A. Ruzsinszky, and J. P. Perdew, *Phys. Rev. Lett.* **115**, 036402 (2015).
 - ¹⁶ A. Togo and I. Tanaka, *Scripta Mater.* **108**, 1 (2015).
 - ¹⁷ G. K. Madsen and D. J. Singh, *Comput. Phys. Commun.* **175**, 67 (2006).
 - ¹⁸ J. M. Skelton, D. Tiana, S. C. Parker, A. Togo, I. Tanaka, and A. Walsh, *J. chem. phys.* **143**, 064710 (2015).
 - ¹⁹ S. S. Shastri and S. K. Pandey, *Comput. Mater. Sci.* **155**, 282 (2018).
 - ²⁰ F. Birch, *Phys. Rev.* **71**, 809 (1947).
 - ²¹ S. S. Shastri and S. K. Pandey, *AIP Conference Proceedings* 2019 (accepted).
 - ²² N. Ashcroft and N. Mermin, *Solid State Physics* (Cengage Learning, 2011).
 - ²³ Y.-S. Kim, M. Marsman, G. Kresse, F. Tran, and P. Blaha, *Phys. Rev. B* **82**, 205212 (2010).
 - ²⁴ K. Gaurav, S. Sisodia, and S. K. Pandey, *J. Renewable Sustainable Energy* **9**, 064703 (2017).
 - ²⁵ A. Togo, L. Chaput, and I. Tanaka, *Phys. Rev. B* **91**, 094306 (2015).
 - ²⁶ C. S. Lue and Y.-K. Kuo, *Phys. Rev. B* **66**, 085121 (2002).
 - ²⁷ C.-S. Lue and Y.-K. Kuo, *J. of Appl. Phys.* **96**, 2681 (2004).
 - ²⁸ J. P. Makongo, D. K. Misra, X. Zhou, A. Pant, M. R. Shabetai, X. Su, C. Uher, K. L. Stokes, and P. F. Poudeu, *J. Am. Chem. Soc.* **133**, 18843 (2011).
 - ²⁹ M. S. Dresselhaus, G. Chen, M. Y. Tang, R. Yang, H. Lee, D. Wang, Z. Ren, J.-P. Fleurial, and P. Gogna, *Advanced materials* **19**, 1043 (2007).